Laser Doppler Velocimetry Investigation of Swirler Flowfields

K. D. Kihm*
Texas A&M University, College Station, Texas 77843
Norman Chigier†
Carnegie-Mellon University, Pittsburgh, Pennsylvania 15213
and
Frank Sun‡
Parker Hannifin Corporation, Cleveland, Ohio 44112

Measurements of three components of mean velocity, turbulent intensities, and Reynolds stress components have been made for the flowfields of swirlers used in gas turbine combustors. The objective is to provide benchmark data for comparison with numerical predictions based on models for turbulent swirling flows and to guide formulation of models that will lead to improved understanding of basic transport processes in reacting and nonreacting swirling flows. An argon-ion laser with Bragg cell frequency shifting was used in the forward scatter mode to obtain velocity measurements. Seeding of the flow through the swirler was provided with a TSI jet atomizer using a glycerol and water mixture (50/50). Swirlers with blade angles of 20, 40, and 60 deg and solidity of 1.17 were carefully machined to provide minimum disturbance to the flow. The number for vanes and the diameter of the hub were changed as the swirl vane angle was changed so that the solidity remained the same. Two supply pressures were used: 750 and 1500 mm H_2O. Data are provided on geometry, reverse flow velocities, and turbulence intensity in the recirculation zones. Turbulence was found to be nearly isotropic. Peak tangential velocities were found at the swirler exit with the 40-deg swirler. This finding is in agreement with the direct force measurements of thrust and torque that were found to be higher for the 40-deg swirler than for the 20- and 60-deg swirlers. The size and strength of the recirculation zone were also found to be highest for the 40-deg swirler.

Nomenclature

d	= diameter of the swirler
G_x	= axial flux of linear momentum
G_ϕ	= axial flux of angular momentum
k	= turbulent kinetic energy $\equiv 1/2(\overline{u'^2}+\overline{v'^2}+\overline{w'^2})$
P	= static pressure
R	= radius of the swirler
r	= coordinate perpendicular to the jet axis
r_h	= hub radius
S	= swirl number
$\bar{u},\bar{v},\bar{w}$	= mean velocities in the x, r, and z directions, respectively
u',v',w'	= turbulent fluctuation velocities in the x, r, and z directions, respectively
$\overline{u'v'},\overline{u'w'}$	= Reynolds stress components
x	= coordinate parallel to the jet axis
z	= coordinate perpendicular to both the jet axis and the r coordinate (the angular direction)
ρ	= density of the air
σ	= solidity
ϕ	= swirl vane angle
ψ	= blockage factor

Introduction

GAS turbine burners consist of a central atomizer through which liquid passes to form a spray surrounded by an annular swirler through which air from the compressor passes into the primary zone of the combustor. There is growing recognition among designers and users of gas turbine engines that the spray and its interaction with the air flowfield can be the root cause of practical problems associated with reduced combustion efficiency, emission of pollutants, radial and circumferential flame nonuniformities, high temperature gas impingement on surfaces, and nonuniform mixing.

For aircraft, requirements are most stringent, and increasing demands are being made on atomizer and swirler performance over all flight conditions likely to be encountered. Much greater effort is being expended on very accurate machining and maintenance of surfaces over which there is flow of liquid and air in order to maintain radial and circumferential symmetry in the spray and jet flows. Detailed measurements have been made separately in air assist sprays of distributions of drop size, drop velocity, and air velocity as a function of nozzle geometry, liquid and air flow rates, and supply pressures.[1,2] There is, however, a strong interaction between the spray and swirler air flow that has not been studied and documented. Clear visual evidence that changes in swirler air flow pattern can cause important changes in spray angle and spray penetration, whereas, conversely, changes in spray pattern cause changes in the swirler air flowfield as a result of entrainment and momentum exchange.[3] An extensive and comprehensive program of research has been initiated to study these interactions and ultimately to demonstrate their influence on combustion performance. This research is expected to influence the design of atomizers and swirlers for gas turbines.

Swirling jets are usually generated by swirlers with hubs to accommodate the fuel injection nozzle. In gas turbine combustion, the air enters the swirler directly from the compressor and after passing through the swirler interacts with the fuel spray. This swirling jet establishes the flowfield that influences atomization and the spray pattern; these have important influences on flame characteristics and combustor performance.

Received Nov. 14, 1988; revision received July 25, 1989.

*Assistant Professor. Mechanical Engineering Department.
†William J. Brown Professor, Mechanical Engineering Department. Associate Fellow AIAA.
‡Senior Research Engineer, Gas Turbine Fuel System Division.

The purpose of this study is to make detailed velocity and turbulence measurements in flowfields generated by angled vane swirlers with different geometries.

The most detailed measurements of swirling jets reported in the literature are for swirl generators with axial-plus-tangential entry. The swirling air emerges from a cylindrical pipe with no disturbance from vanes. Studies also have been made of swirling annular jets. In the earliest studies, velocity was measured by five-hole impact probes, later studies were made with hot-wire anemometers, and some results have been reported on measurements made by laser anemometry. These results are reviewed in books by Beer and Chigier[4] and Gupta et al.[5] as well as in the papers by Chigier and co-workers.[6-8] The design of swirlers and combustors is discussed by Lefebvre[9] and Martin.[10] Fujii et al.[11] used laser Doppler velocimetry to make measurements in swirling jets with and without combustion. Ramos and Sommer[12] used a two-color LDV to measure swirling flow in a research combustor. Sislian and Cusworth[13] measured detailed turbulence characteristics in a strongly swirling free isothermal jet. In furthering our understanding of swirling jets, the following questions are being addressed: 1) What is the basic difference between flowfields in swirling jets when generated by axial flow vane swirlers compared to axial-plus-tangential entry swirl generators? 2) For each type of swirl generator, if the same swirl number is generated, are the jets the same? 3) If not, what additional criteria are required to characterize swirling jets? 4) Does the shape of the initial velocity profiles have an influence on jet behavior? 5) If two jets are generated with the same swirl number but different initial profiles, is the subsequent development of each jet the same or different?

Flame Stabilization by Swirl

When the angular-to-linear momentum ratio exceeds a critical value, a toroidal vortex-type recirculation zone is set up in the central region of the jet close to the burner. This toroidal vortex system plays an important role in flame stabilization since it constitutes a well-mixed zone of hot combustion products that provides a continuous supply of heat and chemically active species to the main flow. Turbulence intensities are high ($\sim 100\%$), allowing high rates of heat and mass transfer by turbulent transport from the recirculation zone to the main stream. Recirculation zones in swirling jets are similar to those produced by bluff bodies, but there are some important differences between the two systems. For bluff bodies, the width and length of the recirculation zones are mainly dependent on the bluff body diameter with some additional influence of the geometric form (forebody geometry) of the bluff body. Recirculation zones in swirling jets are aerodynamic. In the case of hub swirlers, the recirculation zone is governed by the hub diameter at low degrees of swirl; as the degree of swirl is increased, the length of the recirculation zone is progressively increased with little change in the breadth, which remains close to the hub diameter. The reverse flow zone in swirling jets has many of the characteristics of a well-stirred reactor. The temperature and gas composition are almost uniform. This well-stirred zone is fluid dynamically confined by the surrounding flow. The levels of temperature and gas composition within the recirculation zone can be controlled by the amount and nature of the fuel injected into the zone, and the aerodynamic control for mixing and reaction is achieved by varying the degree of swirl. Means are thus available for controlling the rates of formation and reaction of carbon and oxides of nitrogen. Optimum conditions can be found for minimum emission of pollutants.

Several studies comparing burning and nonburning flows show contradictory evidence of the effect of the heat release on turbulence. Gouldin et al.[14] and our previous study[4] of flows with high degrees of swirl and high turbulence intensity showed that heat release results in very little change on the flowfield and turbulence. For a swirl number of 2.2, measured maximum reverse mass flow rates were 80% of input mass flow rate under nonburning conditions and 70% for burning conditions.[4] The enhancement in turbulence due to chemical reaction is so small in comparison to the isothermal turbulence level that it has a negligible effect on the turbulent flowfield.

Recirculation Zone

The determination of the mass flow rates within the recirculation zone is of particular importance for determining the effectiveness of the zone for flame stabilization. Mass flow rates within the reverse flow zone and across the reverse flow zone boundary provide a measure of the strength of the recirculation zone. Boundaries of the reverse flow zone are determined from positions where velocity changes direction from reverse flow to forward flow. Integration of the reverse flow velocity profiles yields the proportion of the main stream fluid that flows back toward the burner. The recirculation eddy is a closed loop, driven by the main stream such that there is no net mass flow across its boundaries. The boundary of the recirculation eddy is determined by radial points at which the forward mass flow equals the reverse mass flow at the axial station. This boundary coincides with the zero streamline that is also determined from integration of the radial distributions of axial velocity. Reverse mass flow rates are determined by

$$m_r = 2\pi \int_0^{r_b} \rho u r \, dr \tag{1}$$

where r_b is the radius at which the axial mean velocity u is equal to zero.

The boundary of the recirculation eddy is larger than that of the reverse flow region, but the boundaries meet at the separation point at the burner exit and at the downstream stagnation point. When the recirculation eddy is not attached to a solid surface, the two boundaries coincide at the forward (upstream) stagnation point. The center or "eye" of the eddies is on the reverse flow boundary. There is no net mass transfer across the reverse flow zone boundary. All heat transfer by convection from the reverse flow zone to the main forward flow stream takes place between the separation edge and the line of the vortex center. In addition to this convective flow, heat and mass are exchanged by turbulent diffusion between the reverse flow and main forward flow. The combustion wave is stabilized within the recirculation eddy where the forward flow velocity is low enough to match the local burning velocity and where there is a continuous supply of heat and chemically active species. This aerodynamic interaction permits a flame to be stabilized over wide ranges of approach flow velocities and mixture ratios.

Bluff Body Effect of Swirler

The flow through the swirler is annular, resulting in recirculation eddies in the wake of the hub. The size of the recirculation zone increases directly with the increase in the diameter of the hub. Flame stabilization could be achieved for low air velocities with mixture ratios near stoichiometric by this hub recirculation zone. As air velocities are increased and as mixture ratios deviate from stoichiometric, it is necessary to strengthen this recirculation zone by introducing swirl into the annular jet. There is general acceptance that recirculation zones are necessary for flame stabilization. As the mass flow rate and the flow velocity are increased, larger and stronger recirculation zones are required to stabilize a flame. The extent to which swirl is needed is not clear. If recirculation zones of the same size and strength are generated by bluff body and swirl, they may be equally effective for flame stabilization. Since air flows through swirlers, fuel and carbon deposition on surfaces is greatly reduced compared to solid face bluff body flame stabilizers.

Design of Swirlers

In the gas turbine industry,[9,10] swirlers have been shown to be effective in controlling the spray angle and placement of

fuel and improving atomization. Both the air and fuel are normally swirled. Swirlers are designed for ease and economy of manufacture as well as for efficiency of operation. Types of swirler that are commonly manufactured are based on 1) drilled circular holes, 2) straight slots, 3) fabricated curved vanes, 4) fabricated straight vanes, and 5) helical slots. The resistance coefficient is dependent on the gap/chord ratio. A cascade of annular axial swirl vanes with a gap/chord ratio resulting in a small resistance coefficient is considered most desirable. When the gap varies with radius, variable chord vanes are used to maintain a constant gap/chord ratio. Pressure drop with curved vanes is lower than with flat vanes. Helical swirlers have blade angles constant with radius independent of rotational angle along the blade.

Blockage factor is defined by

$$\psi = \frac{\text{Total frontal area blocked by thickness of blades}}{\text{Total inlet frontal area with zero thickness}}$$

Solidity is defined by

$$\sigma = \frac{\text{Inlet/frontal swirl vane projected area}}{\text{Total unblocked swirler inlet area}}$$

i.e., "see through" or apparent blockage.

The effectiveness of swirlers can be tested globally by examining the effects of change in swirler design on atomization, spray, and combustor performance. From a fundamental point of view, the purpose of the swirler is to generate a swirling jet that interacts with the spray. More information is, therefore, required on the nature of swirling jets generated by swirlers with different geometries. A wide range of exit axial and swirl velocity profiles can be generated by swirlers. Axial velocity profiles may be uniform, monomodal with a peak near the nozzle outer wall, or multimodal. Swirl velocity profiles can approximate a) solid body rotation with a linear distribution having a peak near the nozzle outer wall, b) a free vortex with a peak near the nozzle inner wall, and c) a Rankine vortex with a solid body core and a free vortex in the outer region. The peak velocity will be between the inner and outer walls of the nozzle.[6] The growth, entrainment, decay, and recirculation of jets with different initial velocity profiles will be significantly different. These differences ultimately influence combustor performance. It would be most useful if correlations could be established between swirler design parameters, including vane angle, number of vanes, curvature, gap size, chord, hub diameter, etc., and swirling jet characteristics. Consideration also must be given to efficiency of swirl generation, defined as kinetic energy in swirling jet divided by the drop in static pressure across swirler × effective flow area through swirler.

Only part of the pressure drops across the swirler reappears as kinetic energy of the subsequent swirling flow. The remainder is "lost" as mechanical energy, but part of it appears as turbulence in the flow.

Swirl Number

The swirler number was first introduced[6] on the basis that the axial flux of linear momentum

$$G_x = 2\pi \int_0^\infty (\rho u^2 + p) r \, dr \tag{2}$$

and the axial flux of angular momentum

$$G_\Phi = 2\pi \int_0^\infty \rho u w r^2 \, dr \tag{3}$$

are conserved along the length of a swirling jet. Also the radial pressure distribution is balanced by the centrifugal forces

$$\frac{dp}{dr} = \rho \frac{w^2}{r} \tag{4}$$

In a more comprehensive theoretical analysis,[7] the governing equations for turbulent axisymmetric swirling flow were integrated using the boundary conditions at the centerline and the jet boundary.

Taking into account the velocity fluctuations, the axial flux of axial momentum becomes

$$G_x = 2\pi \int_0^\infty [\rho(u^2 + \overline{u'^2}) + (p - p_\infty)] r \, dr \tag{5}$$

Integration of the second equation of motion yields

$$\int_0^\infty r(p - p_\infty) \, dr = -\frac{\rho}{2} \int_0^\infty (\overline{w^2} + \overline{w'^2} + \overline{v'^2}) r \, dr \tag{6}$$

Introducing Eq. (6) and Eq. (5)

$$G_x = 2\pi\rho \int_0^\infty [\rho(\overline{u^2} + \overline{u'^2}) - \tfrac{1}{2}(\overline{w^2} + \overline{w'^2} + \overline{v'^2})] r \, dr \tag{7}$$

and the axial flux of angular momentum, including the $x - \phi$ turbulent shear stress term, is

$$G_\Phi = 2\pi\rho \int_0^\infty (\overline{uw} + \overline{u'w'}) r^2 \, dr \tag{8}$$

The swirl number is defined by

$$S_1 = \frac{G_\Phi}{G_x R} \tag{9}$$

This is evaluated by integration of the measured velocity and shear stress profiles at each axial station of the jet. Another criterion for indicating the strength of swirl is based on the ratio of the peak values of swirl and axial velocity at the nozzle exit

$$G = w_{m_o}/u_{m_o} \tag{10}$$

For the special case of solid body rotation flow with a uniform distribution of axial velocity at the orifice

$$S_2 = \frac{G/2}{1 - (G/2)^2} \tag{11}$$

For degrees of swirl higher than 0.4 where the major portion of the fluid leaves the nozzle at the outer edge, the following relation was recommended by Chigier and Chervinsky[7]:

$$S_2 = \frac{G/2}{1 - (G/2)} \tag{12}$$

In the case of a swirler, it has been suggested[4] that the swirler number is only dependent on the swirler geometry. For a swirler with hub diameter d_h, nozzle outer diameter d, and swirl vane angle ϕ,

$$S_4 = \frac{2}{3}\left[\frac{1 - (d_h/d)^3}{1 - (d_h/d)^2}\right] \tan\phi \tag{13}$$

Direct measurement of thrust and torque of the jet gives

$$S_5 = \frac{\text{Torque}}{\text{Thrust } (R)} \tag{14}$$

In previous determinations of swirl number, the outer radius of the nozzle R has been selected as the characteristic length scale for the swirl number. For higher degrees of swirl, the major portion of the flow leaves the orifice near the outer radius of the nozzle.

In this study, we have compared calculations of the five swirl numbers S_1–S_5. S_1 is based on integration of mean and

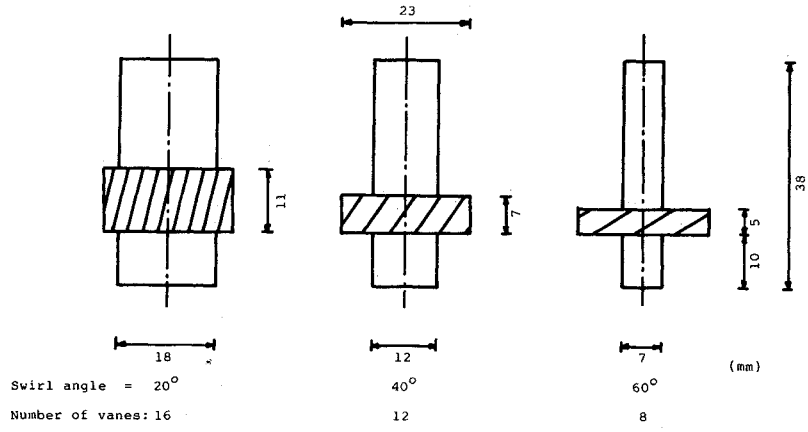

Fig. 1 Air swirler configurations.

fluctuating velocity components. It is very sensitive to the accuracy of the velocity measurements. Near the jet boundary, velocities are low, but because of the large radius, small inaccuracies in velocity measurement can have large influences on the integration. Significant differences can be expected between results reported in this study compared with previous results made by pitot tubes in which no fluctuating velocity components were measured. Furthermore, it has been assumed in the past[7] that the turbulence was isotropic, i.e., $u'_{rms} \sim v'_{rms} \sim w'_{rms}$ so that $\overline{u'^2} - 0.5(\overline{w'^2} + \overline{v'^2}) \approx 0$. Our measurements show that this term is nonzero and can be of the same magnitude or larger than $\overline{u^2} - 0.5\overline{w^2}$.

Swirl number S_2 is based upon the approximation of solid body rotation and uniform axial velocity at the nozzle exit. Our measured profiles show that neither of these approximations is true. This leads to the conclusion that the shape of velocity profiles at the nozzle exit has a strong influence on the jet. Swirl number S_3 was derived by comparison with measurements at higher degrees of swirl (>0.4). There is no reason to believe that this is a generally applicable equation.

In the case of a swirler with fixed vanes, we expect the flow to be guided over the vanes to generate a swirling jet. The swirl angle of the vanes ϕ has the most important influence on generating swirl. As the angle exceeds 40 deg, however, blockage of the flow by the vanes becomes serious, depending upon the number of vanes, and flow separation and stall can occur. The direct measurement of thrust and torque is a global measure of the forces exerted by the jet. The accuracy of these measurements is very dependent on the measurements of load and containment of all the jet. Sufficient information has been obtained in this study to calculate swirl numbers S_1, S_4, and S_5. Because of the different methods used to measure and calculate each of the swirl numbers, they cannot be expected to yield the same results.

Experiments

Swirlers

Figure 1 shows the configuration of flat vane axial swirlers used in this study.[10] All three swirlers have the same outer diameter of 23 mm and are set back 10 mm from the flow exit. The length of the swirlers varies from 11 mm for the 20-deg swirler to 5 mm for the 60-deg swirler, whereas the the hub diameter varies from 18 mm for the 20-deg swirler to 7 mm for the 60-deg swirler. The swirler exit is designed to be located 10 mm behind (upstream from) the nozzle exit. Air flow emerges from the swirler as a series of jets between the individual vanes of the swirler. These individual jets merge in the annular passage between the swirler exit and nozzle exit. Radial and circumferential velocity traverses made at the nozzle exit show that the flow is axisymmetric without a trace of the individual jets that emerge between the vanes. The annular gap width is 5 mm for the 20-deg swirler and 16 mm for the 60-deg swirler.

Table 1 Test conditions

Air pressure: 750 mm H_2O and 1500 mm H_2O
Laser Doppler anemometer:
4-W argon-ion laser with 15 deg off axis in forward detection configuration with Bragg cell frequency modulation
Measurement planes: $x/d = 0.1$, 1, 2, 4, and 8
Measured quantities:
$\bar{u}$, $\bar{v}$, $\bar{w}$, u'_{rms}, v'_{rms}, w'_{rms}, $\overline{u'v'}$, $\overline{u'w'}$, and k
Number of signal counts for each data point = 10,000

These different geometries result in different initial widths for the recirculation zones according to the differences in the hub diameters and in different rates of decay of velocity and turbulence that are a function of the initial annular gap width. The selection of the design parameters of hub diameter, blade angle, swirler blade depth and thickness, and number of blades was based on industrial experience in the design of burners for aircraft gas turbine engines.[10]

Experimental Configuration

The swirlers were mounted vertically with air supplied from a compressor. Pressures were measured upstream from the swirler. The swirler was fitted to the frame of a three-dimensional traversing mechanism that was controlled by computer via dc stepping motors. The air jet was directed vertically downward into stagnant air. A cylindrical wire mesh screen surrounded the air jet to reduce the influence of air currents in the laboratory. Test conditions are given in Table 1. Measurements were made of three components of mean velocity, turbulence intensity, and two components of shear stress. The swirlers were first tested at Parker Hannifin where the direct thrust and torque were measured in a test stand. These results, which are used to calculated swirl number S_5, show that the maximum thrust and torque were generated by the 40-deg swirler.

Laser Anemometer

Velocity measurements were made using a TSI laser Doppler velocimeter operating in the dual-beam, single-component, forward-scatter mode. The principle of orienting wires at 45 deg for making shear stress measurements using hot-wire anemometry is well established (as recommended in the TSI instruction manual). The same principle was adopted for orienting the measurement volume in single-component LDV systems. We and others have shown that there is no significant difference between shear stress measurements made with one- and two-component LDV systems. The transmitting lens had a focal length of 574 mm. The spacing of the interference fringes of green beams in the probe volume was 13.4 μm. The selection of the size of our probe volume had to take into account the upper limit of velocity. For the higher

injection pressure (1500 mm H_2O), the highest frequency filter (TSI 1980 system) together with the frequency modulator of 40 MH_z had to be used to include measurement of velocities up to 120 m/s. With the available optics and electronics of our system, our measurement volume had a length of 2.23 mm (major axis) and a diameter of 0.376 mm (minor axis).

The orientation of the ellipsoidal measurement volume was such that the minor axis coincided with the radial direction of the swirler for the radial (v) and axial (u) velocity component measurements. It was possible to measure the axial (u) component at two different orientations. One of these allowed the minor axis of the ellipsoid to be in the radial direction with better spatial resolution, since the maximum gradients are in this direction. The circumferential (w) velocity component was measured with the minor axis of the probe volume perpendicular to the radial direction. The circumferential (w) component could not be measured with the radially directed minor axis configuration.

The maximum gradients were observed in the exit plane that is at $x/d = 0.1$ and for the 20-deg swirler. The maximum variation of the mean velocity was found to be 34% of the maximum velocity in this plane. In the downstream flow direction, the gradients gradually decreased and the error due to spatial resolution was not as large. In the next plane that is at $x/d = 1$, the maximum variation of velocity was reduced to 26%.

Light scattering from the seed particles in the probe volume was collected in the forward off-axis direction at an angle of 15 deg from the optical axis after passing through a pin hole aperture 0.2 mm in diameter. For on-axis collection, the probe length would have been 19.6 mm. The entire optical system was carefully aligned, calibrated, and rigidly mounted on massive optical tables. The transmitting optics could be rotated 360 deg with respect to the optical axis.

Signals were processed by a TSI 1980 counter-type signal processor with continuous monitoring on a Tektronics 465 oscilloscope. Data reduction was performed on a MINC computer. Average data rates were 3000/s in the central flow and about 500/s at the edges of the flow. For each data point, 10,000 individual realizations were averaged.

The sampling rate of the processor may be limited by the computer buffer, or a time interval between successive measurements can be imposed intentionally so as to provide a saturable detector. Therefore, every particle is not detected, and an approximate constant time interval sampling is achieved. The sampling rate is less than the particle arrival rate.

Particle density = 6×10^{12} particles/m^3 (the generation rate of the TSI six-jet atomizer), and $u = 54$ m/s (maximum axial velocity at the exit).

For an ellipsoidal measurement volume with major and minor axes of 2.23 mm and 0.376 mm, respectively, $A_{ellip} = 6.585 \times 10^{-7}$ m^2 and $3.24 \times 10^{14} \times 6.585 \times 10^{-7} = 2.13 \times 10^8$ particles/s passes through the measurement volume. However, the maximum data rate is 3000 data/s. Although the jet expands further downstream, it is very unlikely that the sampling rate will be higher than the particle arrival rate.

Seeding particles were injected into the air flow from a TSI jet atomizer using 50/50 glycerol and water mixture. The maximum particle diameter at the atomizer outlet reached 8 μm, but less than 1% of the particles had diameters more than 7 μm according to the TSI model 9306 six-jet atomizer instruction manual. The mean diameter is 2 μm at the atomizer outlet, and the arithmetic mean is less than 1 μm at the exit of the 10-ft flexible tubing used to connect the atomizer to the swirler. The size distribution was measured repeatedly using the Aerometrics phase-Doppler particle size analyzer. The maximum particle diameter was found to be about 4 μm. The change in particle size was due to the condensation of larger droplets on the flexible tube wall. Some of the droplets were transported to the space surrounding the jet so that the induced air flow was seeded but at a lower level than the jet flow. This was observed using the laser sheet flow visualization technique.

Errors associated with processing of individual Doppler bursts can arise. Velocity bias was corrected by using a constant time interval sampling mode. Bias associated with nonuniform seeding will affect results near the borders of the jet. Biases associated with incomplete signals and velocity gradients are considered to be small in view of the frequency shift used and the relative smallness of the probe volume. Values of mean velocity components are estimated to be accurate to 4% and turbulence intensities to 8%.

Experimental Results and Discussion

Measurements of mean velocity, turbulent intensities, and shear stress were made at axial distances $x/d = 0.1$, 1, 2, 4,

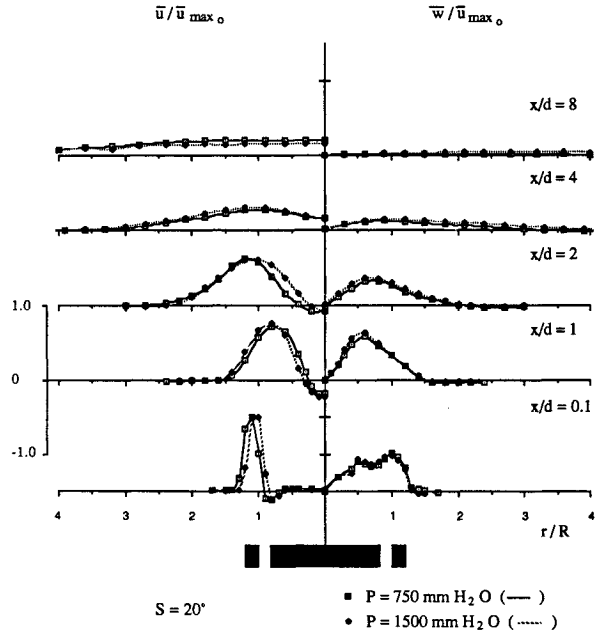

Fig. 2 Axial and tangential mean velocity profiles normalized by the maximum axial velocity at the nozzle exit $\bar{u}_{max_0}$ for the 20-deg swirler: $\bar{u}_{max_0}$ is 54.2 m/s at P = 750 mm H_2O and 87.1 m/s at P = 1500 mm H_2O.

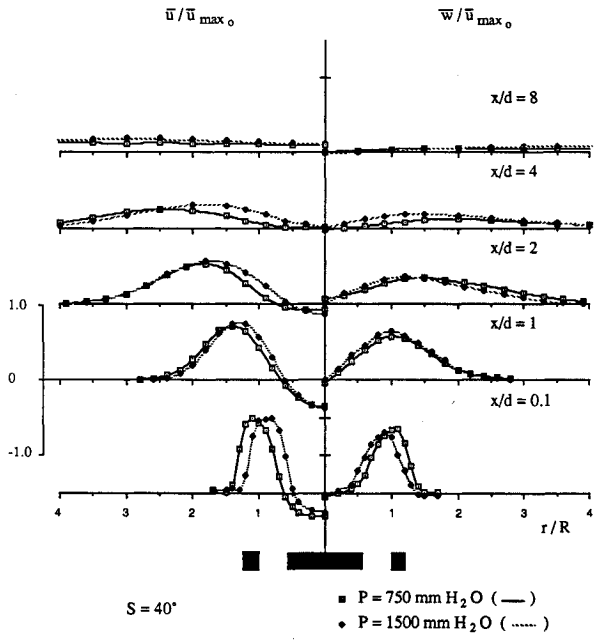

Fig. 3 Axial and tangential mean velocity profiles normalized by the maximum axial velocity at the nozzle exit $\bar{u}_{max_0}$ for the 40-deg swirler: $\bar{u}_{max_0}$ is 54.5 m/s at P = 750 mm H_2O and 65.7 m/s at P = 1500 mm H_2O.

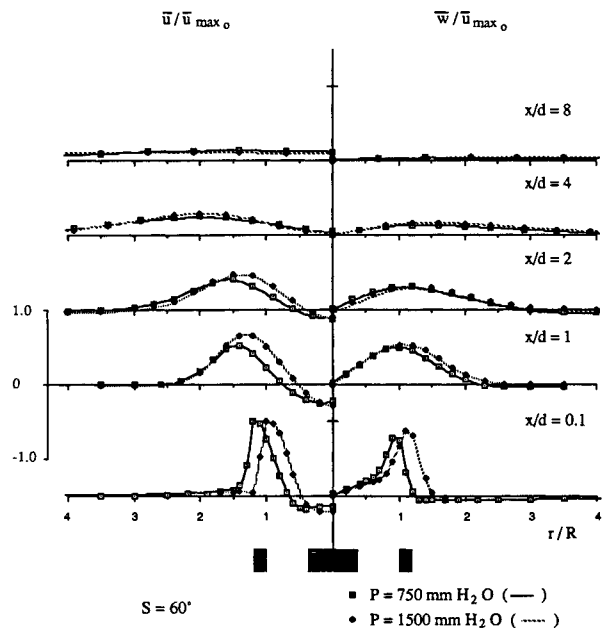

Fig. 4 Axial and tangential mean velocity profiles normalized by the maximum axial velocity at the nozzle exit $\bar{u}_{max_0}$ for the 60-deg swirler: $\bar{u}_{max_0}$ is 47.9 m/s at P = 750 mm H_2O and 65.8 m/s at P = 1500 mm H_2O.

and 8 for swirlers with three blade angles, 20, 40, and 60 deg, and at two supply pressures, 750 and 1500 mm H_2O. Profiles of mean velocity components normalized by the maximum axial velocity component at the nozzle exit ($\bar{u}_{max_0}$) are shown in Figs. 2–4. The axial component profiles show reverse flow (negative velocity) in the central region up to $x/d = 3$. Peak values are off axis. The radial distance of the swirl velocity maximum also increases with the distance downstream.

When the supply pressure is increased from 750 to 1500 mm H_2O, exit velocities are increased by a factor of 1.4. When the data are normalized individually by the maximum axial velocity for each pressure measured at the nozzle exit, there is very close agreement between normalized profiles at the different pressures as shown in Figs. 2–4. This shows that flow patterns are similar at different supply pressures. Jet boundaries and axial spread are essentially the same. Peak velocities are at close but not identical radial locations. Provided that turbulent swirling conditions prevail, it can be expected that this type of similarity will apply for all variations of supply pressure until compressibility begins to influence the flow.

The exit profiles for the supply pressure 750 mm H_2O are compared in Fig. 5. These initial profiles are influenced by the swirler geometry (Fig. 1). The hub diameter decreases from 18 mm at 20 deg to 7 mm 60 deg while the swirler outer diameter remains fixed, so that the annular gap through which the swirling jet emerges is 8 mm for the 60-deg swirler and 2.5 mm for the 20-deg swirler. These differences in swirler geometry have important influences on the near flowfield, the recirculation zone, and jet decay. The axial profiles (Fig. 5a) show that peak values are similar. The reverse flow is highest for the 40-deg swirler. The initial jet width for the 40- and 60-deg swirlers is greater than that for the 20-deg swirler. For the 20-deg swirler, which has the largest ratio of the hub diameter to the nozzle gap width, the jet is not well developed due to the sudden expansion of the flow. This results in a localized recirculation zone (negative velocity region) near the nozzle inner wall, and the axial velocity remains zero in the central region where recirculating flows are not yet established. Initial swirl velocity profiles (Fig. 5b) show that a Rankine-type vortex is formed close to the nozzle exit for the 40- and 60-deg swirlers. The profile has not yet been established for the 20-deg swirler (it does become established further downstream

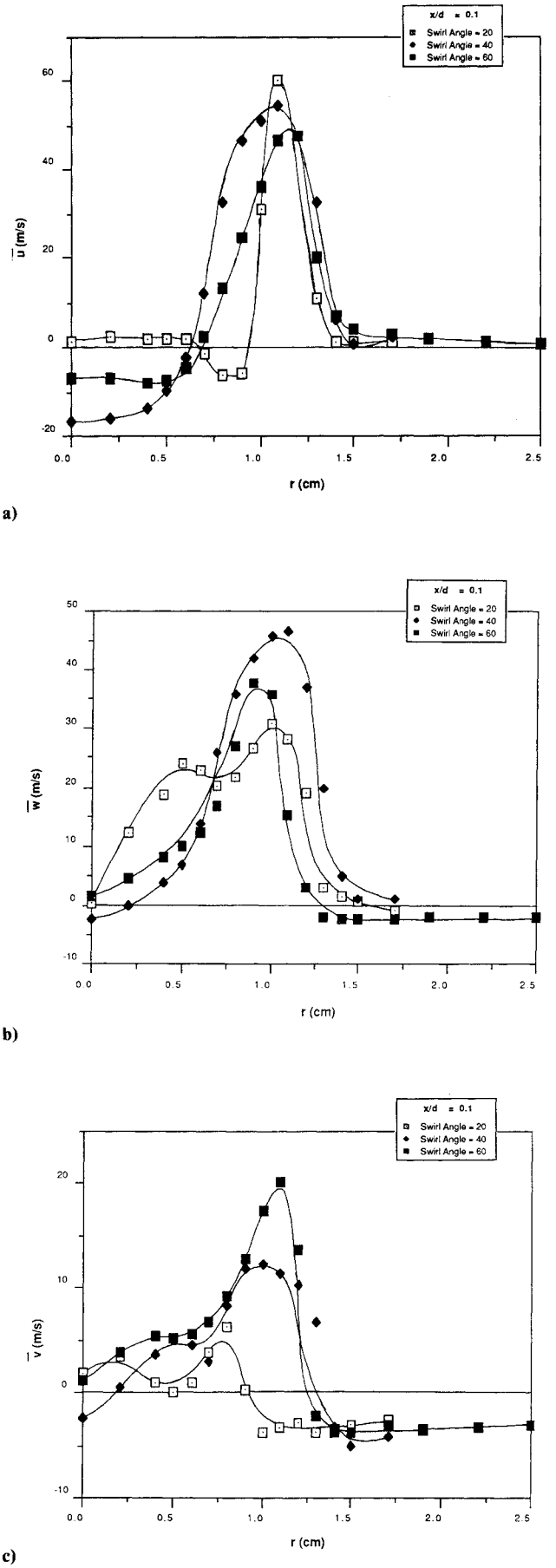

Fig. 5 Mean velocity profiles measured for the three swirlers at x/d = 0.1 and P = 750 mm H_2O: a) axial profiles, b) tangential profiles, and c) radial profiles.

at $x/d = 1$). Peak swirl velocities increase from the 20- to the 40-deg swirler but then decrease for the 60-deg swirler. Peak swirl velocity at the nozzle exit should be most sensitive to an increase in the vane angle of the swirler. The results obtained in this study that exit swirl velocities are lower and the swirl is weaker with the 60-deg swirler than for the 40-deg swirler indicate that the 60-deg swirler needs to be redesigned in order to be more effective. It is believed that this is due to the increased blockage effect of the 60-deg swirler overriding the expected increase in swirl. The initial radial velocity profiles (Fig. 5c) show very low radial velocity components for the 20-deg swirler but a surprisingly high peak of 20 m/s (radially outward) for the 60-deg swirler. This could be a direct influence of the swirler blades directing the jet radially outward, at the expense of not generating high swirl. Negative values outside the nozzle outer walls ($r > 1.2$ cm) are due to the induced air flow by the jet. Entrainment from the surroundings into the jet generates a radial velocity field that has a negative sign, i.e., radially inward, toward the axis. There were sufficient seed particles due to circulation from the jet into the surrounding air to visualize and measure the flow of entrained air.

Seeding particles were found to deposit on the face of the hub. The thickness of the deposit was greatest with the 20-deg swirler (largest diameter hub). This deposit provides some indication of the width of the recirculation zone. The deposition of seeded aerosols was due to a strong internal recirculation of the air. Although there will be no seeded aerosols in real nozzles, fuel droplets could be trapped and deposited onto the hub surface (if any) due to the strong recirculation of the air. This deposit also reflects the probability of deposit of liquid fuel drops, during combustion, on the face of the hub that can lead to carbon formation and growth. For the 60-deg swirler (smallest hub diameter), the degree of swirl is high, and this results in a divergence of the flow as soon as it leaves the nozzle exit. For the 20-deg swirler (large diameter hub and low degree of swirl), the flow, under the influence of the subambient pressure in the hub wake, converges toward the axis, soon after exit from the nozzle. Further downstream the flow diverges. (This can be seen clearly by tracking the peak locations of $\bar{w}/\bar{u}_{\max_0}$ in Fig. 2.) The bimodal initial tangential profile for the 20-deg swirler results in a weak recirculation zone and indicates room for improvement in the design of the swirler.

The centerline axial velocities (Fig. 6) show the extent of the reverse flow from which the length of the recirculation zones (L) can be determined; L/d is 2.3 for the 20-deg and 3.1 for the 40- and 60-deg swirlers. Recirculation zone lengths are influenced both by hub diameter and swirl number. For weak swirl the hub diameter predominates, whereas for strong swirl

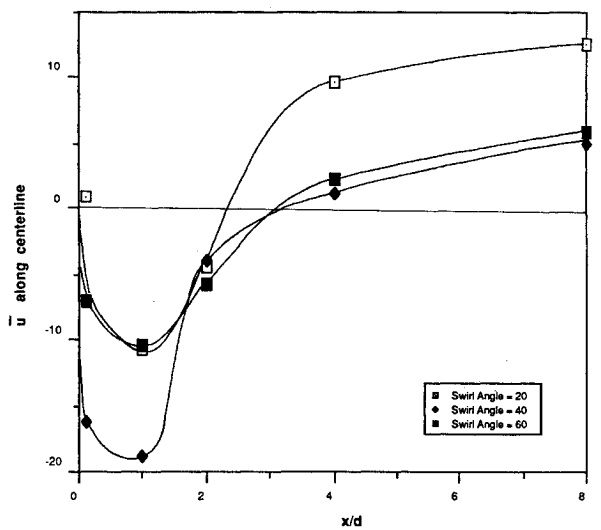

Fig. 6 Axial mean velocity measured along the centerline for the three swirlers at $P = 750$ mm H_2O.

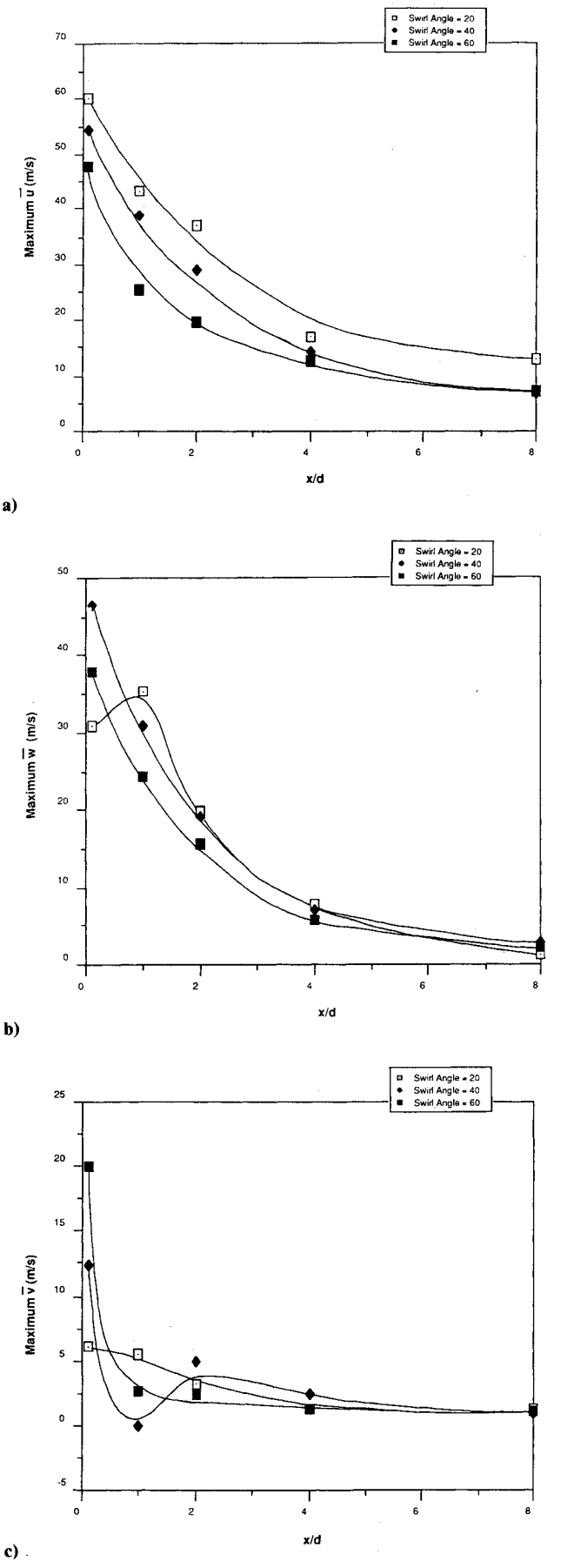

Fig. 7 Decay of maximum mean velocities measured for the three swirlers at $P = 750$ mm H_2O: a) maximum axial mean velocity, b) maximum tangential mean velocity, and c) maximum radial mean velocity.

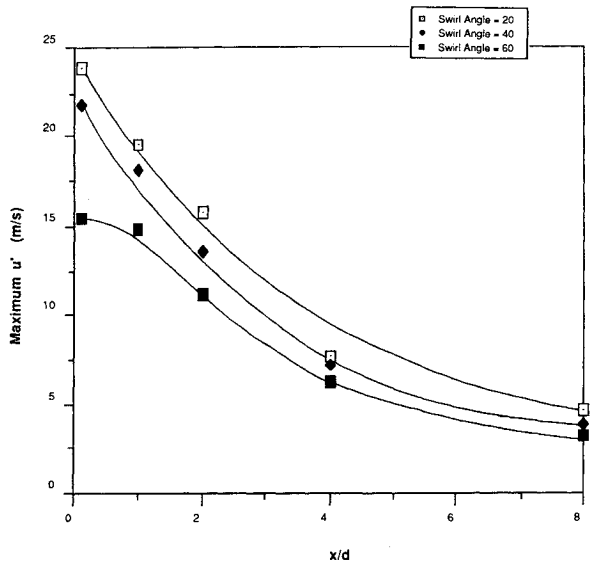

a)

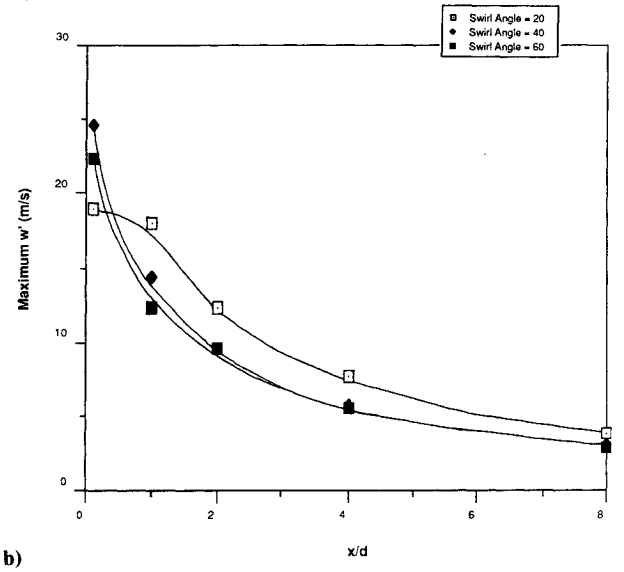

b)

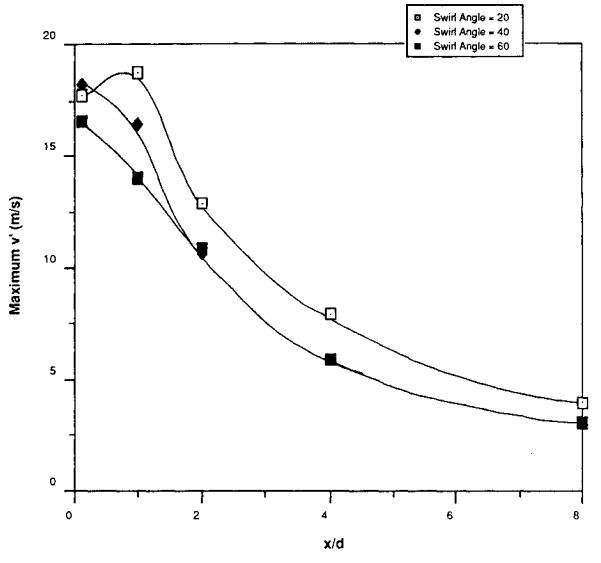

c)

Fig. 8 Decay of maximum rms fluctuating velocity components measured for the three swirlers at P = 750 mm H_2O: a) axial component, b) tangential component, and c) radial component.

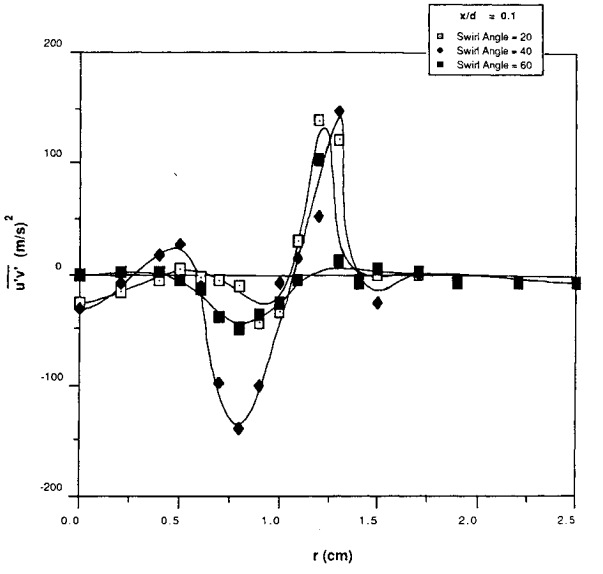

a)

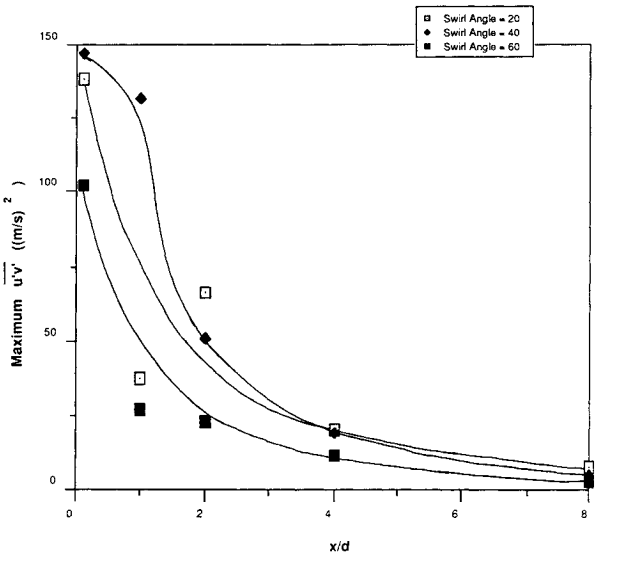

b)

Fig. 9 Reynolds stress component $\overline{u'v'}$ measured at P = 750 mm H_2O; a) $\overline{u'v'}$ at x/d = 0.1, and b) maximum $\overline{u'v'}$ vs x/d.

the swirl number predominates. The peak reverse flow velocity for 40 deg (− 20 m/s) is nearly twice that for the 20- and 60-deg swirlers.

Decay of maximum velocities are shown in Fig. 7. Initial maximum values of $\bar{u}$, $\bar{v}$, and $\bar{w}$ are determined by swirler geometry and exit profiles. These maxima decay downstream, and the rate of decay of $\bar{w}$ (Fig. 7b) is greater than that of $\bar{u}$ (Fig. 7a). For the 20-deg swirler, $\bar{w}_{max}$ shows an increase and then a decrease, having a peak at x/d = 1, while for the 40- and 60-deg swirlers, $\bar{w}_{max}$ decreases continuously along x/d. This is due to the incomplete development of recirculating zones for the case of the 20-deg swirler as previously discussed. At x/d = 8, $\bar{v}$ (Fig. 7c) and $\bar{w}$ have decayed to less than 5% of their initial value for all the cases. The maximum $\bar{v}$ at x/d = 0.1 increases with an increase of swirl angle.

Decay of maximum fluctuating components of velocity is shown in Fig. 8. The magnitudes of the three components of fluctuating velocity are similar, and their rates of decay are similar. Each jet can be considered to be close to local isotropic turbulence; i.e., fluctuations have the same magnitude in all directions at a particular point in the flow. The results show, surprisingly, that the axial fluctuating velocity components are highest for 20-deg and lowest for the 60-deg

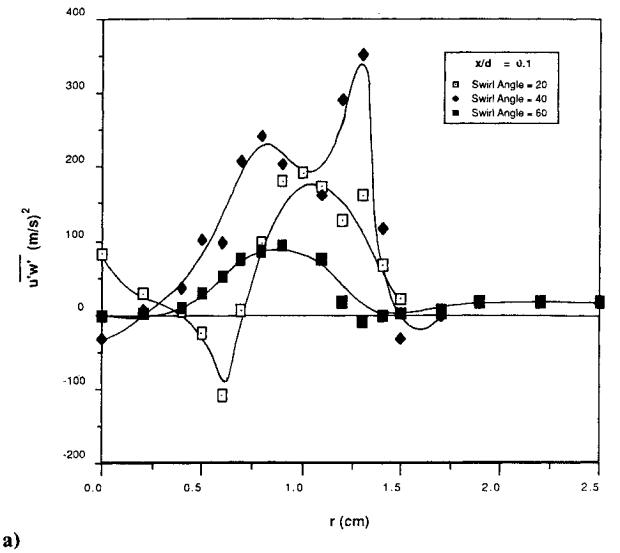

a)

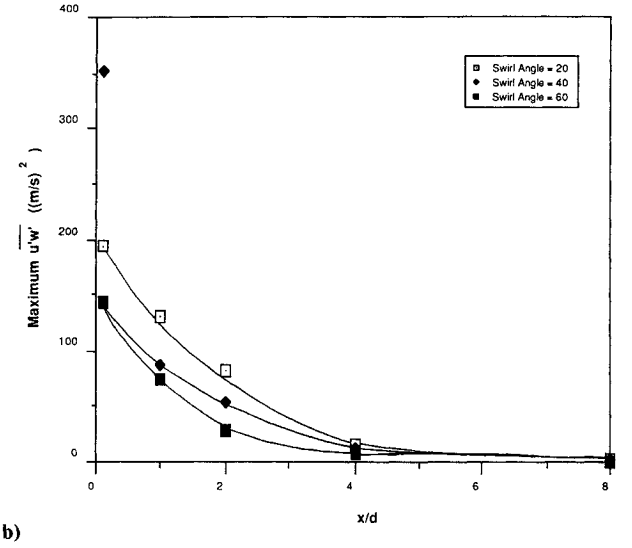

b)

Fig. 10 Reynolds stress component $\overline{u'w'}$ measured at P = 750 mm H_2O; a) $\overline{u'w'}$ at x/d = 0.1, and b) maximum $\overline{u'w'}$ vs x/d.

swirler. This is contrary to expectation since it has been assumed that the addition of tangential shear to axial shear and the stronger recirculation zone in jets with strong swirl would result in higher turbulence for the jet with the higher degree of swirl.

Figure 9a shows the profile of the axial Reynolds stress term $\overline{u'v'}$. This is the turbulent shear stress component that would be generated in a jet even if there was no swirl. It has both negative and positive values associated with the positive and negative gradients of the mean velocity profiles. For swirling flows, the turbulent shear stress distribution is strongly nonisotropic and is a function of the degree of swirl and position in the flowfield.[8] Both positive and negative peaks are greatest for the 40-deg swirler, indicating that the degree of swirl for the 40-deg swirler is the highest. Figure 9b shows the decay of the axial shear. The decay is rapid so that there is very little shear remaining at $x/d = 8$ where the axial mean velocity gradients become negligible. The magnitudes for the 60-deg swirler are lower than for the 20- and the 40-deg swirlers.

Figure 10a shows the profile of tangential shear. Magnitudes (positive) of $\overline{u'w'}$ are higher than $\overline{u'v'}$, showing that tangential shear plays a significant role in the swirling flowfield. Tangential shear for 40 deg is nearly double for the 20- and 60-deg swirlers, again showing that the 40-deg swirler generates the highest swirl. The maxima of tangential shear shown in Fig. 10b demonstrates faster decay than those of axial shear.

The kinetic energy of turbulence is determined from the fluctuating velocity components that were found to be close to local isotropy. The decay of maxima of k (Fig. 11) shows little difference between the three swirlers.

Integration of the profiles of measured mean and fluctuating components of velocity yields the axial flux of axial momentum G_x and the axial flux of angular momentum G_ϕ [Eqs. (6) and (7)] at each axial station. For the calculation of the swirl number, the average of the inner and outer radius of the swirler, $(r_h + R)/2$, was selected. It has been argued that since a major portion of the flow is concentrated near the outer radius of the swirler, the swirler outer radius R is a more suitable characteristic length for the swirl number calculation. However, the effect of the inner radius (or, equivalently, the hub radius) on the swirling flow is as important as the effect of the outer radius as we have seen in the case of the 20-deg swirl flow. The values of S_1 computed from the measurements are shown in Fig. 12 at each axial station for each swirler.

In examining these results, account needs to be taken of the sensitivity of the integrations to the accuracies of 1) measurement of velocity, 2) averaging, 3) positioning of probe volume, 4) symmetry of jet, and 5) assessment of jet boundary. All velocities approach zero at the jet boundary. It is difficult to ascertain the exact location of the jet boundary, and it is usual to designate a boundary at a "cut off" of the velocity profile at 10% or 5% of the peak measurement. Small variations of the location of the jet boundary together with uncertainties in the measurement of small velocities at large radii have significant effects on integrated quantities. Even though, in principle, both axial and angular momentum should be conserved, it is difficult to prove this from velocity measurements. Nozzle exit velocity profiles should provide more accurate results because velocity magnitudes are highest and boundaries can be more accurately specified. Farther downstream velocities have lower magnitudes and boundaries can be determined with lower accuracies. Far downstream, velocities are so low that they can be influenced by small outside disturbances, and it is very difficult to find the jet boundary.

It is most interesting to compare the swirl numbers determined from direct measurements of thrust and torque S_5, as measured by Parker Hannifin, with swirl numbers determined from integrated velocity measurements S_1. Swirl numbers of 0.45 for the 20-deg swirler and 1.0 for the 40-deg swirler seem appropriate as averaged values. The integrated velocity shielded $S_1 = 0.65$ at the nozzle exit compared to the torque/thrust $S_5 = 1.3$ for the 60-deg swirler. The swirl number calcu-

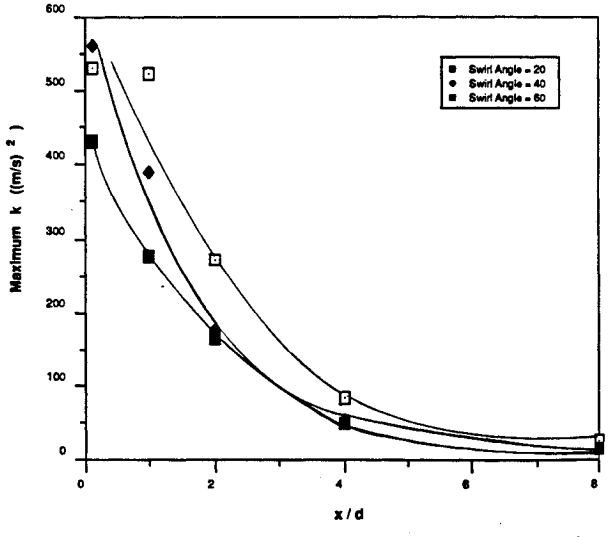

Fig. 11 Decay of kinetic energy along x/d measured at P = 750 mm H_2O for the three swirlers.

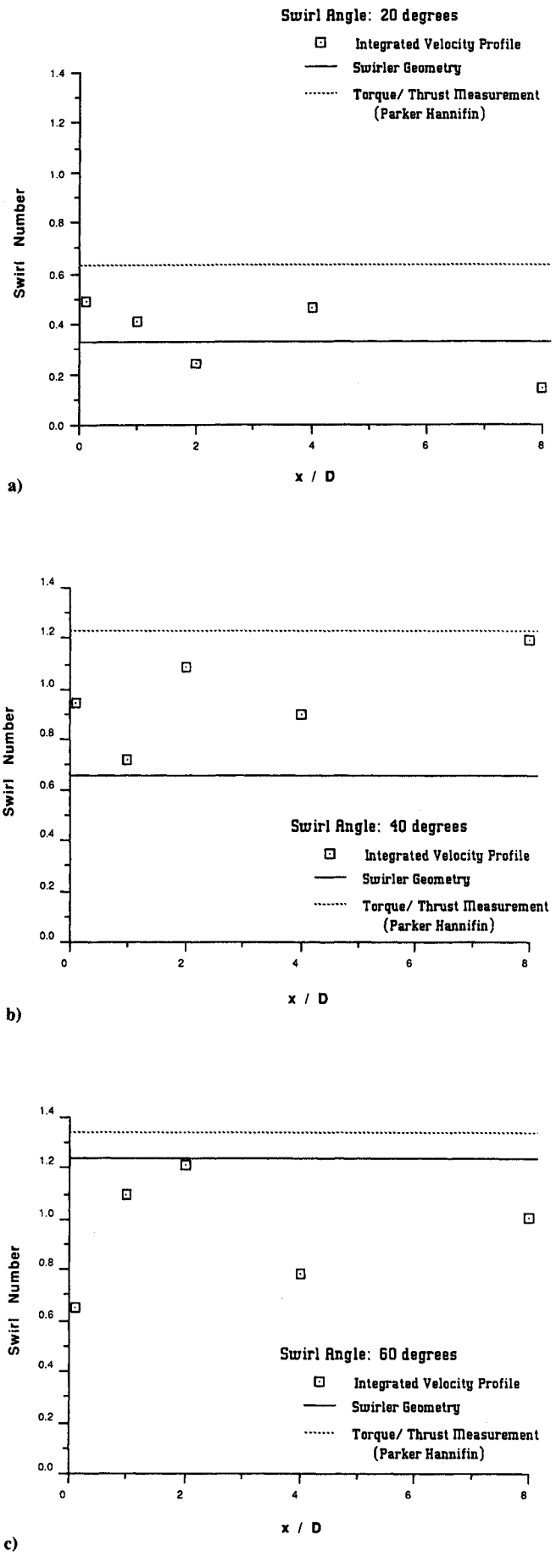

Fig. 12 Swirl numbers S_1, S_4, and S_5 at P = 750 mm H_2O: a) swirl angle = 20 deg, b) swirl angle = 40 deg, and c) swirl angle = 60 deg.

lated from the swirler geometry (principally the vane angle) does not take into account any blockage or flow separation effects. (It would yield the highest swirl number for a vane of 90 deg, when no flow could pass through the swirler.) For this reason, the calculated value of S_4 is too high for the 60-deg swirler. Although each type of swirl number is calculated on a different basis using different measurements and different assumptions, a reasonably fair agreement was found between the different calculated swirl numbers.

Conclusions

Using a laser Doppler velocimeter, detailed measurements of mean and turbulent velocity components and turbulent shear stress components have been made for the jet flows of 20-, 40-, and 60-deg swirlers for 750 and 1500 mm H_2O supply air pressure conditions. The main conclusions reached are listed as follows:

1) When the mean velocity components $\bar{u}$, $\bar{v}$, and $\bar{w}$ are normalized based on the maximum axial velocity at the nozzle exit, there is very close similarity between normalized profiles at different supply pressures for each swirler.

2) The recirculation zone, which depends on the degree of swirl and the geometry of swirlers, is not well established near the nozzle exit for the case of high ratio of the inner to the outer radius of the swirler r_h/R and of low degree of swirl. This can create a serious deposition problem of fuel droplets onto the hub surface under the influence of subambient pressure in the hub wake.

3) The measurements of turbulent velocity components demonstrate that each jet can be considered to be close to local isotropic turbulence except at the nozzle exit where the magnitudes and the decay of the fluctuations strongly depend on flow directions.

4) The distributions of the turbulence shear stress components $\overline{u'v'}$ and $\overline{u'w'}$ are strongly anisotropic, and both positive and negative peaks are greatest for the 40-deg swirler, indicating that the degree of swirl for the 40-deg swirler is the highest.

5) For the 20- and 40-deg swirlers, swirl numbers determined from integrated velocity measurements S_1 showed close agreement with both S_4 determined from the swirler geometry and S_5 determined from torque/thrust measurements. However, for the 60-deg swirler, S_4 and S_5 significantly deviate from S_1, giving larger values than S_1. This discrepancy is believed to be due to the increased blockage effect with the large vane angle that was not considered in determining S_4.

Acknowledgment

The authors gratefully acknowledge the financial assistance and encouragement of this research by the Parker Hannifin Corporation.

References

[1]Yule, A. J., Ah Seng, C., Felton, P. G., Ungut, A., and Chigier, N. A., "Sprays, Drops, Dusts, Particles," *Combustion and Flame*, Vol. 44, 1982, pp. 71-84.

[2]Mao, C.-P., Wang, G., and Chigier, N. A., "The Structure and Characterization of Air-Assisted Swirl Atomizer Sprays," *Atomisation and Spray Technology*, Vol. 2, No. 2, 1986, pp. 151-169.

[3]Chigier, N. A., *Energy, Combustion and Technology*, McGraw-Hill, New York, 1981, pp. 1-16, 100-150.

[4]Beer, J. M., and Chigier, N. A., *Combustion Aerodynamics*, Applied Science, 1972, pp. 100-146.

[5]Gupta, A. K., Lilley, D. G., and Syred, N., *Swirl Flows*, Abacus, 1984.

[6]Chigier, N. A., and Beer, J. M., "Velocity and Static Pressure Distribution in Swirling Air Jets Issuing from Annular and Divergent Nozzles," *Journal of Basic Engineering*, Vol. 4, 1964, pp. 788-796.

[7]Chigier, N. A., and Chervinsky, A., "Experimental Investigation of Swirling Vortex Motion in Jets," *Journal of Applied Mechanics, Transactions of ASME*, Series E34, 1967, pp. 443-451.

[8]Lilley, D. G., and Chigier, N. A., "Nonisotropic Turbulent Shear Stress Distribution in Swirling Flows from Mean Value Distributions," *International Journal of Heat and Mass Transfer,* Vol. 14, 1971, pp. 573-585.

[9]Lefebvre, A. H., *Gas Turbine Combustion,* Hemisphere, Washington, DC, 1983.

[10]Martin, C. A., "Aspects of the Design of Swirlers as Used in Fuel Injectors for Gas Turbine Combustors," American Society of Mechanical Engineers, New York, Paper 87-GT-139, June 1987.

[11]Fujii, S., Eguchi, K., and Gomi, M., "Swirling Jets With and Without Combustion," *AIAA Journal,* Vol. 19, No. 11, 1981, pp. 1438-1442.

[12]Ramos, J. I., and Sommer, H. T., "Swirling Flow in a Research Combustor," *AIAA Journal,* Vol. 23, No. 2, 1985, pp. 241-247.

[13]Sislian, J. P., and Cusworth, R. A., "Measurements of Mean Velocity and Turbulent Intensities in a Free Isothermal Swirling Jet," *AIAA Journal,* Vol. 24, No. 2, 1986, pp. 303-309.

[14]Gouldin, F. C., Depsky, J. S., and Lee, S.-L., "Velocity Field Characteristics of a Swirling Flow Combustor," *AIAA Journal,* Vol. 23, No. 1, 1985, pp. 95-102.